Available online at www.sciencedirect.com
SCIENCE DIRECT
Tetrahedron
Tetrahedron 62 (2006) 4408–4418

Efficient synthesis and structural analysis of new dioxopiperazine isoquinolines

Nuria Cabedo,[a] Noureddine El Aouad,[a] Inmaculada Berenguer,[a] Miguel Zamora,[b] M. Carmen Ramírez de Arellano,[c] Fernando Suvire,[b] Almudena Bermejo,[a,†] Daniel Enriz[b] and Diego Cortes[a,*]

[a]*Laboratorio de Farmacognosia, Departamento de Farmacología, Facultad de Farmacia, Universidad de Valencia, 46100 Burjassot, Valencia, Spain*
[b]*Departamento de Química, Universidad Nacional de San Luis, Chacabuco 917, 5700 San Luis, Argentina*
[c]*Departamento de Química Orgánica, Facultad de Farmacia, Universidad de Valencia, 46100 Burjassot, Valencia, Spain*

Received 22 September 2005; revised 21 February 2006; accepted 21 February 2006

Available online 20 March 2006

Abstract—We report herein the synthesis of new dioxopiperazine isoquinolines using the Pictet–Spengler cyclisation. Our synthetic strategy for the preparation of two new compounds (**5**, **6**), with a tetrahydro-6*H*-pyrazino[1,2-*b*]isoquinoline-1,4-dione moiety was developed in only four steps. To understand better the crucial step of the synthesis reported here, theoretical calculations using semiempirical (PM3), ab initio and DFT computations were carried out on a reduced system model. The structure of chlorohydrate water solvate of tetrahydro (2-piperidinylethyl)-6*H*-pyrazino [1,2-*b*]isoquinoline-1,4-dione (**6**·HCl·2H_2O) was determined by X-ray diffraction. Theoretical calculations (RHF/3-21G and RB3LYP/6-31G(d)) were also performed for compound **6** neutralised with a chloride ion.

1. Introduction

Substituted 1,2,3,4 isoquinolines represent a class of natural and synthetic compounds that has received considerable attention because of their significant and powerful biological activities, including antitumor, antibiotic and anticonvulsant properties.[1–4] In many studies aimed at developing simple and efficient syntheses of polyfunctional heteroaromatic fused isoquinolines,[5] it has been reported that the exact structure of the reaction compounds could not be established unequivocally, because several closely similar isomeric products could be formed.[6,7]

In the present paper, as a part of our search for new polyfunctional heterocycles,[8,9] we report the synthesis of two new tetrahydro-6*H*-pyrazino[1,2-*b*]isoquinoline-1,4-diones. The rigid framework of these triclyclic compounds incorporates both L-phenylalanine and piperazine-2,5-dione bones using Pictet–Spengler cyclisation. We have introduced a flexible linker into the molecule bearing basic nitrogen as a means of improving aqueous solubility. We describe a short and convenient method in the asymmetric total synthesis of this type of compounds that may be of potential use for the construction of several functionalised piperazine isoquinoline derivatives and will serve as building blocks for natural products.[3] To know better the alkylation–cyclisation step of the synthesis reported here, theoretical calculations using semiempirical (PM3), ab initio and density functional theory (DFT) computations were carried out on a reduced system model. Structure elucidation of the new products was established by spectroscopy and X-ray crystallography. In addition, geometrical optimisations using both RHF/3-21G and RB3LYP/6-31G(d) calculations were performed for tetrahydro (2-piperidinylethyl)-6*H*-pyrazino[1,2-*b*]isoquinoline-1,4-dione (compound **6**) neutralised with a chloride ion with the aim to compare these computations with the experimental results.

2. Results and discussion

2.1. Synthesis

Our approach is based on the use of Pictet–Spengler cyclisation, reaction that was readily adaptable to preparing

Keywords: Dioxopiperazine isoquinolines; Synthesis; Pictet–Spengler; X-ray; Semiempirical (PM3); Ab initio and DFT calculations.
* Corresponding author. Tel.: +34 963 54 49 75; fax: +34 963 54 49 43; e-mail: dcortes@uv.es
† Current address: Departamento de Citricultura, IVIA, Carretera Moncada-Náquera Km 4.5, 46113 Moncada, Valencia, Spain.

0040–4020/$ - see front matter © 2006 Elsevier Ltd. All rights reserved.
doi:10.1016/j.tet.2006.02.065

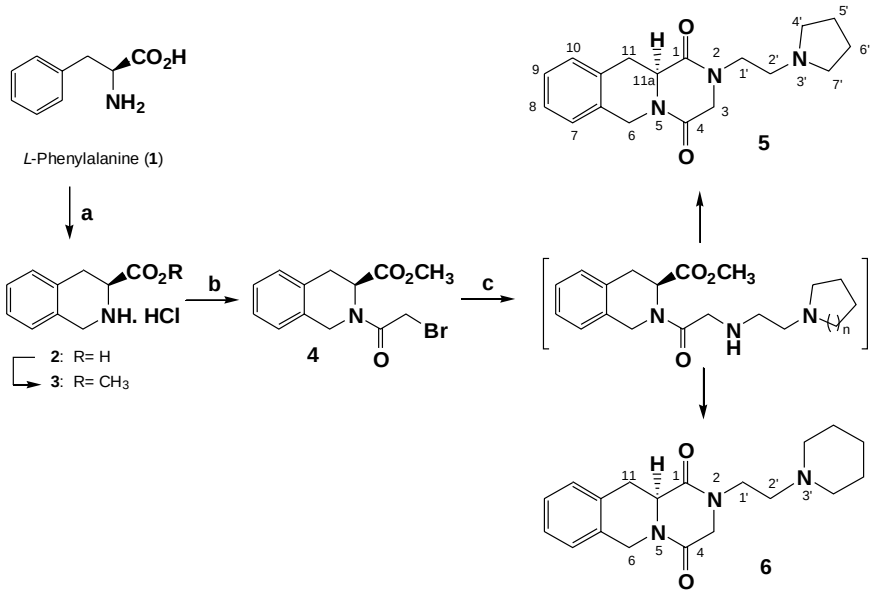

Scheme 1. Reagents and conditions: (a) (i) HCHO/37% HCl, 95 °C, 3 h 30 min; (ii) MeOH, concd H_2SO_4, rt, 2 h; (30%); (b) $BrCOCH_2Br$, Et_3N, CH_2Cl_2, 0 °C to rt, 3 h (65%); (c) 1-(2-aminoethyl) pyrrolidine or 1-(2-aminoethyl)piperidine, K_2CO_3, CH_2Cl_2, reflux, 4 h (49% for **5** and 57% for **6**).

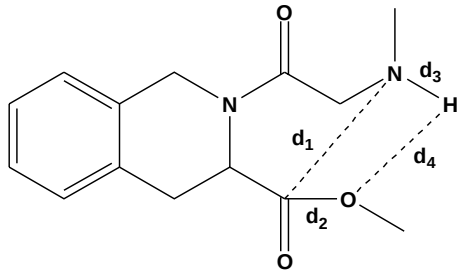

Scheme 2. Reduced model employed to simulate the alkylation–cyclisation process, showing the critical distances d_1, d_2, d_3 and d_4.

substituted 1,2,3,4 isoquinolines.[10] Our synthetic strategy for the obtention of two new compounds with a tetrahydro-6*H*-pyrazino[1,2-*b*]isoquinoline-1,4-dione motif (**5** and **6**), was developed in only four steps (Scheme 1).

As shown, the starting material L-phenylalanine, unsubstituted on the phenyl ring, was chosen as chiral synthon in the construction of these tetrahydroisoquinoline derivatives. Thus, the amino acid (**1**) was condensed with formaldehyde in the presence of 37% HCl through a Pictet–Spengler cyclisation to form the corresponding tetrahydroisoquinoline 3-carboxylic acid, **2**.[11] Fischer esterification of **2**

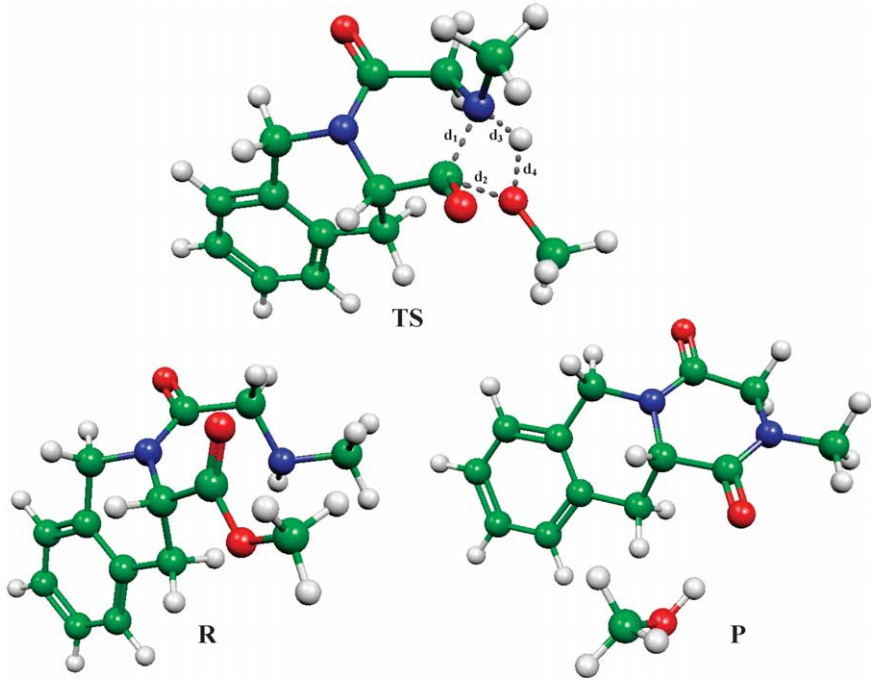

Figure 1. RB3LYP/6-31++G(d,p) optimised geometries of the **R**, **TS** and **P** species. The critical interatomic distances (d_1, d_2, d_3 and d_4) are denoted in the **TS** structure.

Table 1. Absolute energy (Hartrees), ZPE and selected interatomic distances (in Å) for **R**, **TS** and **P** obtained at four different levels of theory

	R						**TS**						**P**			
	d_1(C–N)	d_2(C–O)	d_3(N–H)	d_4(O–H)	ZPE[a]	Energy[b]	d_1(C–N)	d_2(C–O)	d_3(N–H)	d_4(O–H)	ZPE[a]	Energy[b]	d_1(C–N)	d_4(O–H)	ZPE[a]	Energy[b]
RPM3	3.2411	1.3714	0.9983	3.1359	0.301166	0.154138	1.5580	2.2263	1.1137	1.5743	0.297266	0.230009	1.4219	0.9503	0.299940	0.127293
RHF/6-31G(d)	2.7734	1.3206	1.0022	3.8871	0.334195	−873.798579	1.5083	2.1368	1.0573	1.5641	0.331551	−873.711906	1.340	0.951	0.332148	−873.820268
RB3LYP/6-31G(d)	2.7480	1.3496	1.0189	3.8883	0.310578	−879.195706	1.5673	1.9988	1.1588	1.3830	0.306233	−879.142514	1.3548	0.9779	0.309381	−879.217963
RB3LYP/6-31++G(d,p)	2.7575	1.3491	1.0178	3.8801	0.308766	−879.256720	1.5619	1.9934	1.1465	1.3935	0.304681	−879.206621	1.3529	0.9761	0.307591	−879.284985

Note that d_2 and d_3 distances are broken bonds in **P**.
[a] ZPE: zero-point correction (Hartree/particle).
[b] Sum of electronic and zero-point energies (Hartree).

Table 2. Selected interatomic distances, RMS gradient and relative energies obtained for the different steps of RHF/6-31G(d) IRC calculations

	R	Step 1	Step 2	Step 3	Step 4	**TS**	Step 5	Step 6	Step 7	Step 8	**P**
d_1 (Å)	2.84564	1.63727	1.58800	1.55364	1.52802	1.50828	1.49039	1.47075	1.44784	1.42215	1.33921
d_2 (Å)	1.32393	1.55005	1.69054	1.85012	2.00375	2.13677	2.23566	2.28991	2.31531	2.35812	3.24820
d_3 (Å)	1.00003	1.00141	1.00593	1.01716	1.03155	1.05732	1.11020	1.22108	1.37514	1.54342	3.15195
d_4 (Å)	3.01654	1.83646	1.77164	1.71428	1.64998	1.56406	1.44288	1.28427	1.12102	1.00359	0.95019
RMS gradient (Hartree/bohr)	5.81×10^{-5}	3.07×10^{-3}	3.18×10^{-3}	2.05×10^{-3}	8.23×10^{-4}	2.93×10^{-5}	9.11×10^{-4}	3.88×10^{-3}	7.49×10^{-3}	6.04×10^{-3}	3.06×10^{-6}
ΔE (kcal/mol)	0.00	35.92	42.32	47.61	50.40	51.16	50.39	46.20	34.42	20.48	−16.56

The optimised values of these parameters obtained for **R** and **P** are also included for comparison. The total energy of **R** (−874.124984907 Hartree) was taken as reference value.

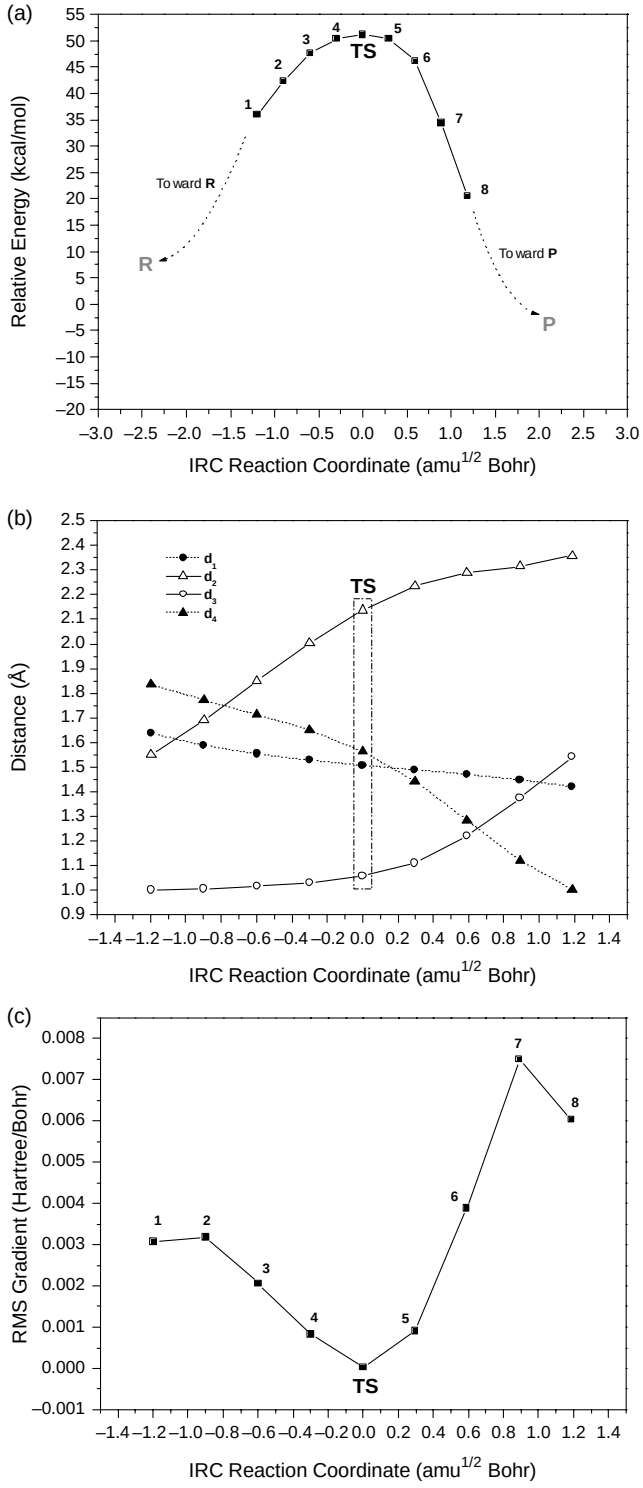

Figure 2. RHF/6-31G(d) IRC calculations showing, respectively. Relative energies (a), interatomic distances (b) and RMS gradient (c) versus the IRC coordinates.

provided a stable tetrahydroisoquinoline methyl carboxylate **3**. N-acylation of the ester, which was carried out by treatment with bromoacetyl bromide at room temperature with 1.5 equiv of triethylamine in dichloromethane afforded the amide **4**.[12] In a crucial last step, **4** was reacted with primary amines such as 2-pyrrolidinylethylamine and 2-piperidinylethylamine under standard conditions.[13] A spontaneous alkylation–cyclisation reaction proceeded

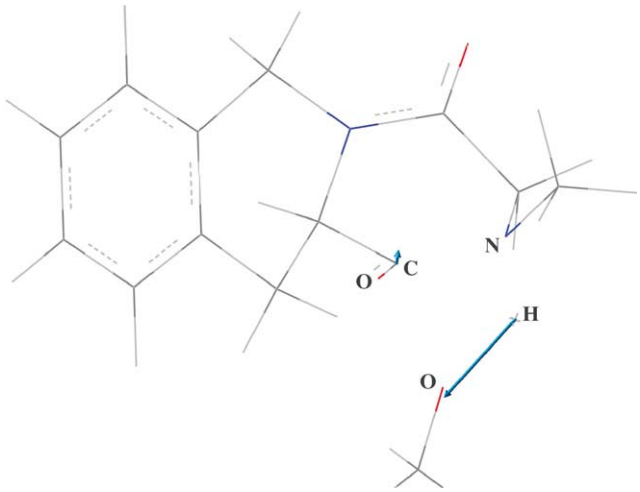

Figure 3. Molecular geometry and the result of the vibrational analysis of the transition state obtained from RB3LYP/6-31++G(d,p) calculations. The length of each arrow is proportional to the degree of vibration of the atom.

affording the tetrahydro (2-pyrrolidinylethyl)-6*H*-pyrazino[1,2-*b*]isoquinoline-1,4-dione derivative **5** and its homologue 2-piperidinylethyl **6**, respectively. Compound **6**·HCl was subjected to single crystal X-ray analysis and the experimental results were compared with ab initio RHF/3-21G and B3LYP/6-31G(d) calculations (see Section 2.3). The X-ray structure determination revealed that the carbon C-12 has the same configuration as in the starting material.

2.2. Alkylation–cyclisation reaction

Formation of tricyclic compounds (**5** and **6**) suggested that the mechanism operating in this transformation involved the spontaneous cyclisation, rationalised by considering that the conformation of **4** adopts a boat-like conformer in which the ester and the amide are proximal in pseudo-equatorial orientations allowed for easy approach of the amino group on the ester carbonyl. To understand better this one-pot reaction, we conducted a computer-assisted study simulating the alkylation–cyclization process. The purpose was to obtain more precise information about this mechanism of reaction.

A reduced model (NCH_3 instead of *N*-piperidinylethyl moiety) (see Scheme 2) was used to perform the theoretical calculations. The use of a reduced model to calculate the PES and to simulate the reaction mechanism is convenient since compounds **5** and **6** are too large for accurate quantum mechanic calculations. When choosing the model compound, the ability to reproduce electronic properties of the entire molecules **5** and **6** were considered.

The critical points (**R**, **TS** and **P**) were obtained using different levels of theory: semiempirical (PM3), ab initio (restricted Hartree–Fock calculations with the basis set 6-31G(d)) and DFT (RB3LYP/6-31G(d)) computations. In addition, to improve our results, we optimise these critical points using an extended basis set including diffuse and polarisation functions (RB3LYP/6-31++G(d,p)). The differences between the geometries obtained at the RB3LYP/6-31G(d) and RB3LYP/6-31++G(d,p) levels

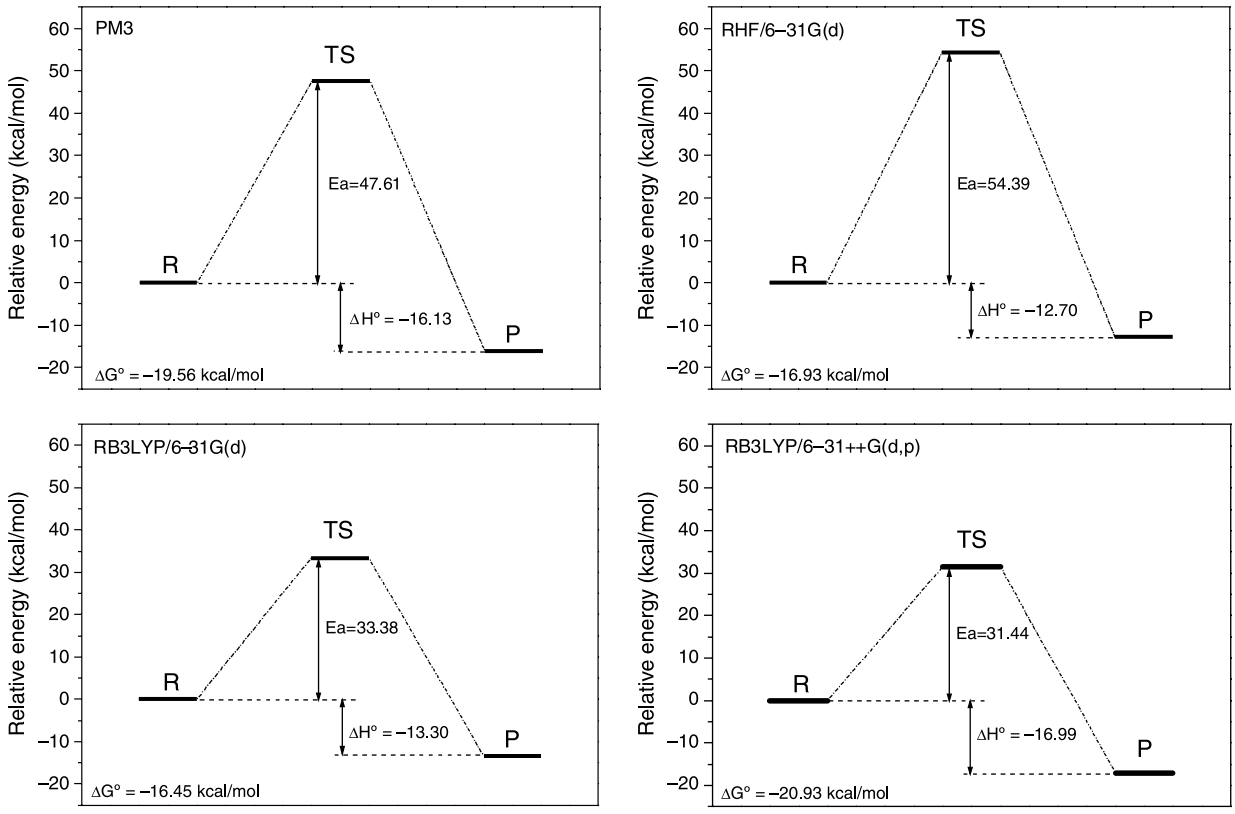

Figure 4. Schematic diagram of the potential energy surface showing the possible mechanism for the alkylation–cyclisation calculated at four different levels of theory. $T=298.15$ K and $P=1$ atm.

are almost negligible. The differences between bond lengths are smaller than 0.01 Å and bond angles show agreement within 0.5°. However, some differences were observed for the activation energy, $\Delta_r H^\circ$ and $\Delta_r G^\circ$ values.

The optimised geometries of **R**, **TS** and **P** calculated at RB3LYP/6-31++G(d,p) level have been collected in Table S1 (Supplementary material) and a spatial view of these structures is shown in Figure 1. Selected interatomic distances for **R**, **TS** and **P** are listed in Table 1.

To determine if the transition state connects to the desired reactant and products, we traced the reaction path from the **TS** to the **R** and **P**, respectively. Thus we calculate the RHF/6-31G(d) intrinsic reaction coordinates (IRC), which formed the path that should be followed by a particle moving along the steepest descent paths with an infinitesimal step from the **TS** down to both the reactant and the product sides on the PES. In order to verify the true minimum, we optimised the last IRC point to the next local minimum. In the forward RHF/6-31G(d) IRC calculations, the last IRC point was obtained at a C–N distance (d_1) of 1.42 Å and an O–H distance (d_4) of 1.00 Å. RHF/6-31G(d) IRC calculations in backward direction showed that the last IRC point was obtained at a C–N distance of 1.63 Å and an O–H distance of 1.83 Å (see Table 2). Figure 2a–c summarises the results obtained from the RHF/6-31G(d) IRC calculations showing, respectively, the relative energies, distances and RMS gradient versus the IRC coordinates.

The characterisation of the **TS** showed that the structure has only one negative eigenvalue. The calculated vibrational frequency (i876.47 cm^{-1} at RB3LYP/6-31++G(d,p) level) showed that the eigenvector that corresponds to the imaginary frequency is primarily a translation of the hydrogen (*N*–H) towards the oxygen atom (d_4 spatial orientation in Scheme 2). This result might be well appreciated in Figure 3. In addition, in this figure we can also observe a lower degree of vibration between the *O* and C atom (in the carbonyl group of ester moiety). It should be noted that in the transition state structure, the nitrogen atom (*N*–H group) is rotated toward the carbon atom (carbonyl group) in order to form the new C–*N* bond in **P**. The course of the cyclisation is characterised by the approach of *N* to C (d_1 in Scheme 2). Further approach of the *N* to *C* along the pathway, raises the energy of the complex until it reaches a transition state (**TS**) at a *C*–*N* distance of 1.5619 Å (at RB3LYP/631++G(d,p) level). Along this path of approach, this state has the characteristics of a real transition state, with a single negative eigenvalue, in the Hessian matrix of force constants. From this transition state the complex moves down the potential energy surface to produce **P**, which is the product of the alkylation–cyclisation.

All the frequencies obtained for the **TS** structure using DFT (RB3LYP/6-31G(d) and RB3LYP/6-31++G(d,p)) calculations are given in Table S2 in the Supplementary material.

The potential energy diagram along the reaction coordinate calculated at four different levels of theory is schematically drawn in Figure 4. As outlined in Section 4.3 barrier heights have been corrected by ZPE (zero-point energies) using the ZPE values summarised in Table 1. Reaction enthalpies are

Table 3. Geometrical parameters obtained for compound **6** from X-ray, ab initio (RHF/3-21G) and DFT (B3LYP/6-31G(d)) calculations

Bond	Bond length (Å)			Internal angle	Angle (°)			Torsional angle	Angle (°)		
	X-ray	RHF	DFT		X-ray	RHF	DFT		X-ray	RHF	DFT
O(4)–C(4)	1.233	1.219	1.253	C(1)–N(2)–C(3)	123.6	119.7	120.2	C(1)–N(2)–C(1′)–C(2′)	−105.3	−105.8	−106.1
O(1)–C(1)	1.238	1.227	1.259	C(1)–N(2)–C(1′)	121.2	120.0	120.0	C(3)–N(2)–C(1′)–C(2′)	70.5	72.2	70.1
N(2)–C(1)	1.330	1.352	1.368	C(3)–N(2)–C(1′)	115.1	120.0	119.7	C(8′)–N(3′)–C(2′)–C(1′)	−179.3	−178.4	−178.5
N(2)–C(3)	1.452	1.470	1.478	C(2′)–N(3′)–C(8′)	108.8	109.4	109.7	C(4′)–N(3′)–C(2′)–C(1′)	57.8	56.5	55.7
N(2)–C(1′)	1.467	1.453	1.462	C(2′)–N(3′)–C(4′)	113.6	114.0	114.2	N(2)–C(1′)–C(2′)–N(3′)	66.7	59.5	60.2
N(3′)–C(2′)	1.497	1.508	1.512	C(8′)–N(3′)–C(4′)	110.0	111.1	111.4	C(2′)–N(3′)–C(4′)–C(5′)	179.7	−178.7	−178.8
N(3′)–C(8′)	1.497	1.520	1.527	C(4)–N(5)–C(12)	125.5	120.2	120.5	C(8′)–N(3′)–C(4′)–C(5′)	57.5	57.1	56.2
N(3′)–C(4′)	1.498	1.518	1.523	C(4)–N(5)–C(6)	118.4	119.1	118.6	N(3′)–C(4′)–C(5′)–C(6′)	−57.5	−57.9	−56.6
N(5)–C(4)	1.335	1.350	1.364	C(12)–N(5)–C(6)	114.5	120.2	120.6	C(4′)–C(5′)–C(6′)–C(7′)	56.0	57.7	55.5
N(5)−C(12)	1.458	1.473	1.487	N(2)–C(1′)–C(2′)	113.5	113.6	114.6	C(5′)–C(6′)–C(7′)–C(8′)	−55.2	−56.7	−54.7
N(5)–C(6)	1.473	1.475	1.483	N(3′)–C(2′)–C(1′)	115.8	115.1	115.5	C(2′)–N(3′)–C(8′)–C(7′)	177.6	176.0	176.5
C(1′)–C(2′)	1.521	1.538	1.538	N(3′)–C(4′)–C(5′)	110.9	109.9	110.4	C(4′)–N(3′)–C(8′)–C(7′)	−57.4	−57.2	−56.1
C(4′)–C(5′)	1.520	1.533	1.533	C(6′)–C(5′)–C(4′)	110.5	111.4	112.0	C(6′)–C(7′)–C(8′)–N(3′)	56.2	57.0	55.5
C(5′)–C(6′)	1.510	1.536	1.539	C(5′)–C(6′)–C(7′)	110.8	109.2	109.9	C(1)–N(2)–C(3)–C(4)	−2.7	−46.3	−41.5
C(6′)–C(7′)	1.516	1.537	1.539	C(8′)–C(7′)–C(6′)	110.5	110.8	111.6	C(1′)–N(2)–C(3)–C(4)	−178.5	−135.8	−142.3
C(7′)–C(8′)	1.505	1.532	1.532	N(3′)–C(8′)–C(7′)	112.1	110.9	111.3	C(12)–N(5)–C(4)–O(4)	−172.3	−173.1	−175.0
C(3)–C(4)	1.487	1.520	1.522	N(2)–C(3)–C(4)	117.5	109.9	111.7	C(6)–N(5)–C(4)–O(4)	−7.7	−0.2	−0.9
C(1)–C(12)	1.507	1.516	1.526	O(4)–C(4)–N(5)	123.2	124.4	124.0	C(12)–N(5)–C(4)–C(3)	8.8	7.1	4.4
C(12)–C(11)	1.530	1.532	1.538	O(4)–C(4)–C(3)	118.8	122.3	121.2	C(6)–N(5)–C(4)–C(3)	173.4	−179.9	178.5
C(11)–C(14)	1.503	1.511	1.511	N(5)–C(4)–C(3)	118.1	113.3	114.8	N(2)–C(3)–C(4)–O(4)	176.8	−139.9	−143.1
C(6)–C(13)	1.500	1.512	1.510	O(1)–C(1)–N(2)	122.2	123.2	122.7	N(2)–C(3)–C(4)–N(5)	−4.2	39.8	37.4
C(14)–C(13)	1.391	1.389	1.408	O(1)–C(1)–C(12)	117.7	123.0	122.1	C(3)–N(2)–C(1)–O(1)	−177.2	−176.3	−175.8
C(14)–C(10)	1.399	1.382	1.400	N(2)–C(1)–C(12)	120.0	113.8	115.2	C(1′)–N(2)–C(1)–O(1)	−1.6	1.7	0.4
C(10)–C(9)	1.362	1.385	1.399	N(5)–C(12)–C(1)	114.8	108.4	110.4	C(3)–N(2)–C(1)–C(12)	5.3	3.5	2.3
C(9)–C(8)	1.389	1.383	1.400	N(5)–C(12)–C(11)	109.2	110.0	110.5	C(1′)–N(2)–C(1)–C(12)	−179.2	−178.5	178.5
C(8)–C(7)	1.394	1.385	1.399	C(1)–C(12)–C(11)	110.8	111.1	111.7	C(4)–N(5)–C(12)–C(1)	−6.2	−49.4	−43.1
C(7)–C(13)	1.393	1.382	1.400	C(14)–C(11)–C(12)	111.9	108.9	110.2	C(6)–N(5)–C(12)–C(1)	−171.3	137.7	143.0
				N(5)–C(6)–C(13)	112.3	111.0	112.3	C(4)–N(5)–C(12)–C(11)	−131.2	−171.1	−167.1
				C(13)–C(14)–C(10)	118.5	119.7	119.6	C(6)–N(5)–C(1)–C(11)	63.6	16.0	19.0
				C(13)–C(14)–C(11)	121.2	116.9	117.4	O(1)–C(1)–C(12)–N(5)	−178.9	−137.5	−143.0
				C(10)–C(14)–C(11)	120.3	123.3	123.0	N(2)–C(1)–C(12)–N(5)	−1.2	42.7	38.8
				C(9)–C(10)–C(14)	120.8	120.3	120.4	O(1)–C(1)–C(12)–C(11)	−54.6	−16.5	−19.6
				C(10)–C(9)–C(8)	121.1	120.0	120.0	N(2)–C(1)–C(12)–C(11)	123.1	163.7	162.2
				C(9)–C(8)–C(7)	118.9	119.9	119.9	N(5)–C(12)–C(11)–C(14)	−48.3	−55.0	−53.5
				C(13)–C(7)–C(8)	120.0	120.1	120.3	C(1)–C(12)–C(11)–C(14)	−175.6	−175.1	−178.0
				C(14)–C(13)–C(7)	120.6	120.1	119.9	C(4)–N(5)–C(6)–C(13)	150.4	−141.4	−148.1
				C(14)–C(13)–C(6)	121.9	117.4	118.4	C(12)–N(5)–C(6)–C(13)	−43.3	31.5	25.9
				C(7)–C(13)–C(6)	117.5	122.4	121.7	C(12)–C(11)–C(14)–C(13)	17.5	47.5	44.1
								C(12)–C(11)–C(14)–C(10)	−161.6	−131.5	−135.0
								C(13)–C(14)–C(10)–C(9)	−2.8	0.6	0.8
								C(11)–C(14)–C(10)–C(9)	176.3	179.6	179.8
								C(14)–C(10)–C(9)–C(8)	2.2	−0.5	−0.7
								C(10)–C(9)–C(8)–C(7)	−0.5	−0.1	0.0
								C(9)–C(8)–C(7)–C(13)	−0.6	0.6	0.6
								C(10)–C(14)–C(13)–C(7)	1.7	−0.2	−0.1
								C(11)–C(14)–C(13)–C(7)	−177.4	−179.1	−179.2
								C(10)–C(14)–C(13)–C(6)	−178.8	−179.2	−178.3
								C(11)–C(14)–C(13)–C(6)	2.1	1.8	2.6
								C(8)–C(7)–C(13)–C(14)	0.0	−0.4	−0.6
								C(8)–C(7)–C(13)–C(6)	−179.6	178.6	177.5
								N(5)–C(6)–C(13)–C(14)	9.5	−41.7	−38.1
								N(5)–C(6)–C(13)–C(7)	−170.9	139.3	143.8

moreover corrected for thermal energy calculated at 298.15 K. Inspection of the collected data in Figure 4 indicates that the barrier heights are sensitive to the employed theory level. Thus, PM3 and RHF/6-31G(d) calculations predict an activation energy of 47.61 and 54.39 kcal/mol, whereas RB3LYP/6-31G(d) and RB3LYP/6-31++G(d,p) calculations suggest 33.38 and 31.44 kcal/mol, respectively. Analysis of the DFT data indicates that enlarging the basis set (from 6-31G(d) to 6-31++G(d,p)) increases the stability of the transition state structure by 1.94 kcal/mol. It is interesting to note that the free energy of activation of the reaction at the highest level of theory is 31.44 kcal/mol, an indicative value of which the reaction can be carried out at room temperature at a reasonable rate.

The reaction enthalpies ($\Delta_r H^\circ$) for the alkylation–cyclisation calculated within the different approaches employed in this study are summarised in Figure 3. In contrast with the features found in the barrier height analysis, the calculated values are quite similar at the different levels of theory. Our theoretical results strongly suggest that the alkylation–cyclisation is an exothermic process ($\Delta_r H^\circ = -17.13$ kcal/mol at RB3LYP/6-31++G(d,p) level), which is in agreement with our experimental data. It occurs if the reagent can assume the proper orientation. The proposed reaction mechanism with four-centre **TS** that has been characterised, as described previously, is a true reaction path that shows to be reasonable according to the estimated activation energy.

The E_a, $\Delta_r H^\circ$ and $\Delta_r G^\circ$ values obtained from DFT calculations for the alkylation–cyclisation could explain the spontaneous nature of this process. However, it should be noted that our theoretical calculations had been performed for a reduced model system in vacuum; therefore caution is needed in these interpretations, because the complete molecular systems as well as solvent effects could change somewhat these results.[14]

2.3. Crystal structure analysis

The solid state structure of **6**·HCl·2H$_2$O was determined by single crystal X-ray diffraction (Table 3, Fig. 5). Crystal structure confirms the absolute configuration (*S*) on *C*(12) which is in accordance with the starting material, L-phenylalanine. The three fused rings are not coplanar and present a half-folded conformation. The plane formed by the aromatic ring C7–C8–C9–C10–C13–C14 and C6 and C11 (mean deviation 0.019 Å) makes a dihedral angle of 33.7(2)° with the C1–N2–C3–C4–N5–C12 ring plane (mean deviation 0.029 Å). The piperidine ring adopts the chair conformation with the flexible connecting chain in the equatorial position. The bond lengths of *N*(3′)–C(2′) (1.497(5) Å), *C*(2′)–*C*(1′) (1.519(6) Å) and *C*(1′)–*N*(2) (1.469(5) Å) show the C–*N* and C–C single bond character. The ammonium hydrogen atom is acting as hydrogen bond donor to the chloride atom (N3′···Cl1 3.159(4) Å, H3′···Cl1 2.26 Å, N3′-H3′···Cl1 168.3°). Other hydrogen bonds have been found involving the two water solvated molecules hydrogen atoms and the carbonyl or the water oxygen atoms or the chloride ion (O5–H5A···O1 163(5)°, O5···O1 2.793(5) Å, H5A···O1 1.92(2); O5–H5B···O4^{i} 166(5)°, (i) $-x+1$, $y-1/2$, $-z+1/2$, O5···O4^{i} 2.812(5) Å, H5B···O4^{i} 1.94(2) Å; O6–H6D···Cl1 131(5)°, O6···Cl1 3.249(6) Å, H6D···Cl1 2.60(5) Å; O6–H6C···O5^{ii} 161(6), (ii) $-x+1$, $y+1/2$, $-z+1/2$, O6···O5^{ii} 2.874(7) Å, H6C···O5^{ii} 2.02(4) Å).

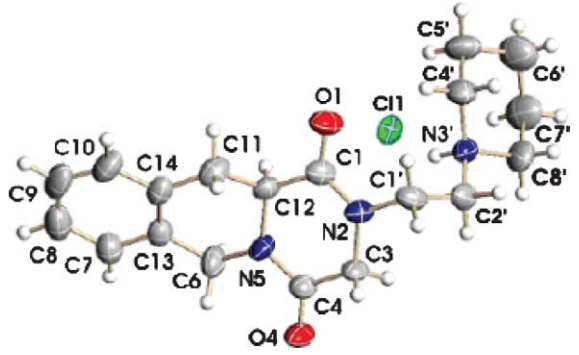

Figure 5. X-ray ellipsoid plot of the cation of **6**·HCl (H$_2$O molecules have been removed for a better view of the crystal structure).

We were also interested to learn whether the experimentally obtained structure of **6**·HCl·2H$_2$O could also be reproduced with reasonable agreement by standard computational methods. Thus we calculate compound **6** neutralised with a chloride (Cl^-) ion. To perform these optimisations we chose as starting geometry the conformation obtained from X-ray where the chloride was located at an arbitrary C–*N*H distance of 3.07 Å. The *z*-matrix of the optimised geometry at the B3LYP/6-31G(d) level is given in Table S3 the supplementary material. In order to obtain information about the electronic aspects, we calculate the molecular electrostatic potential (MEP) using RB3LYP/6-31G(d) calculations. A spatial view of the MEP obtained for compound **6** neutralised with a chloride Cl^- is shown in Figure 6.

The geometry optimisations have been carried out at the restricted Hartree–Fock (RHF) level with 3-21G basis set and RB3LYP/6-31G(d) level of theory. Table 3 gives the main geometrical parameters for the RHF/3-21G and DFT optimised geometries. Both levels of calculations well reproduce the bond distances and angles observed at X-ray even when periodical conditions were not considered in our calculations. Agreements between the calculated structures and the experimentally determined X-ray crystal structure were excellent; a strikingly significant correlation $R=0.99904$ (RHF/3-21G) and $R=0.99911$ (B3LYP/6-31G(d)) was found between the bond lengths optimised at both levels of theory and those obtained from X-ray. The experimentally determined bond lengths are slightly shorter than those observed in the DFT calculated geometry. These differences in bond lengths may be due to the short intermolecular contacts in the crystal. Inspection of Figure 7 reveals the similarity between the X-ray, RHF/3-21G and RB3LYP/6-31G(d) geometries. Specifically, only minute deviation was found between torsion angle values found at X-ray when compared to those found at RHF/3-21G or at RB3LYP/6-31G(d) levels; being the main difference the spatial position of the piperidine ring (see Table 2). The different environments, that is, crystal versus isolated molecule may yield differences between both experimental and theoretical structures due to the role played by

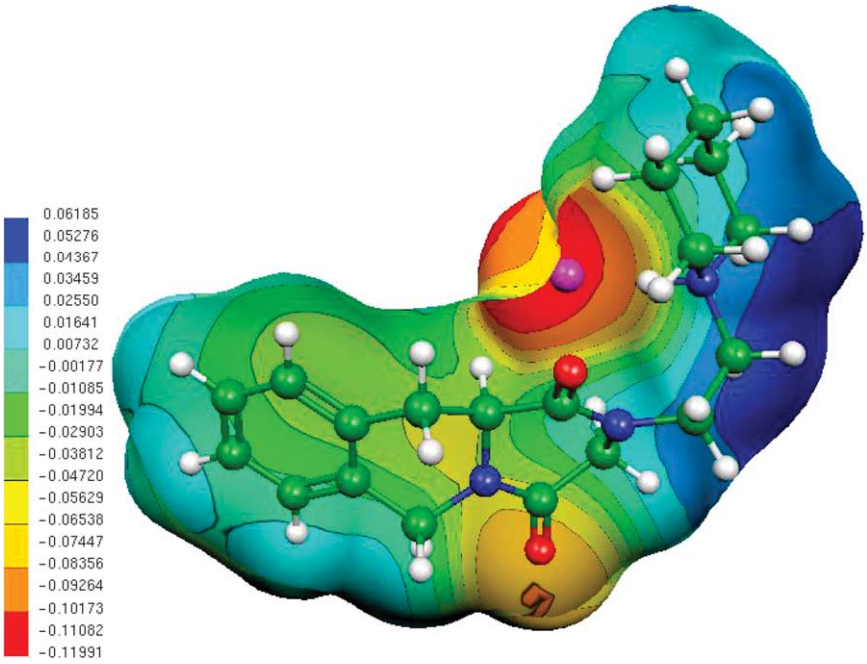

Figure 6. Electrostatic potential-encoded electron density surfaces of the core structures of compound **6** interacting with a chloride ion. The surfaces were generated using RB3LYP/6-31G(d) calculations. The coloring represents electrostatic potential with red indicating the strongest attraction to a positive point charge and blue indicating the strongest repulsion. The electrostatic potential is the energy of interaction of the positive point charge with the nuclei and electrons of a molecule. It provides a representative measure of overall molecular charge distribution.

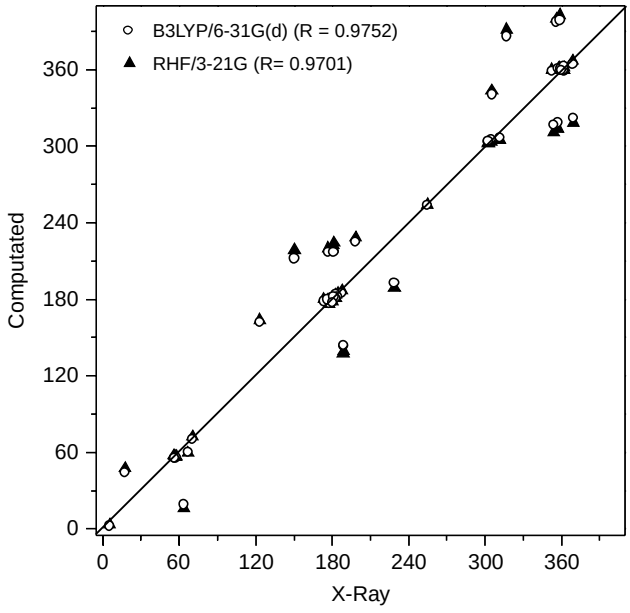

Figure 7. A graph showing the correlation between the torsional angles of compound **6** optimised at RHF/3-21G and B3LYP/6-31G(d) versus torsional angles obtained from X-ray analysis.

the intermolecular forces. However, it is clear that there is a complete agreement between theoretical calculations and experimental data. Comparisons between Figures 5 and 6 illustrate well this situation.

3. Conclusions

A selective and easy route to tetrahydro-6*H*-pyrazino-[1,2-*b*]isoquinoline-1,4-dione from L-phenylalanine via the Pictet–Splenger reaction, N-acylation followed by alkylation–cyclisation, was developed. Our results indicate that semiempirical and ab initio calculations combined with RB3LYP/6-31++G(d,p) computations can well interpret the crucial step of the title reaction. The molecular structure of **6** neutralised with a chloride ion was optimised using RHF/3-21G and B3LYP/6-31G(d) calculations and compared with experimental data to assess the accuracy of the theoretical methods. Both levels of calculations are in agreement with the X-ray data.

4. Experimental

4.1. General

Optical rotations were determined with a Perkin-Elmer 241 polarimeter. IR spectra (film) were run on a Perkin-Elmer 1750 FTIR Spectrometer. EIMS, LSIMS and HREIMS were determined on a VG Auto Spec Fisons instrument, and electrospray ionisation (LC-MSD, API-Electrospray positive) was determined on a Hewlett-Packard (HP-1100). NMR spectra were recorded on Bruker AC-250, Varian Unity-300 or Varian Unity-400 spectrometer at 250, 300 or 400 MHz for ^{1}H, and 75 or 100 MHz for ^{13}C. Multiplicities of ^{13}C NMR signals were assigned by DEPT experiments. COSY 45, HSQC and HMBC correlations were recorded at 400 MHz. All reactions were monitored by analytical TLC with silica gel 60 F_{254} (Merck 5554). The residues were purified through 60 H silica gel column (5–40 μm, Merck 7736), and by flash chromatography (230–400 μm, Merck 9385).

4.1.1. (*S*)-Methyl-1,2,3,4-tetrahydroisoquinoline-3-carboxylate hydrochloride (3). A suspension of L-phenylalanine (**1**, 500 mg, 3.0 mmol) and formaldehyde (1 mL of

a 37% aqueous solution) in concd HCl (5 mL) was heated for 30 min at 95 °C. Then concd HCl (1 mL) and formaldehyde (0.5 mL) were added and the mixture was heated at 95 °C for another 3 h. The mixture reaction was allowed to cool to room temperature overnight and the solid was filtered and washed with H_2O. Then, the residue of THIQ **2** hydrochloride was dissolved in hot MeOH (10 mL), treated with concd H_2SO_4 (0.2 mL) and shaken at room temperature for 2 h. The solvent was concentrated under reduced pressure to give 204 mg of the methyl ester hydrochloride **3** (0.9 mmol, 30%) as a white solid, which was used directly in the next step.

^{1}H NMR (300 MHz, $CDCl_3$) δ: 2.86 (br s, 1H, NH), 2.91 (dd, J=16.2, 10.2 Hz, 1H, CH_2-4a), 3.05 (dd, J=16.2, 4.8 Hz, 1H, CH_2-4b), 3.71 (dd, J=10.2, 4.8 Hz, 1H, CH-3), 3.73 (s, 3H, OCH_3), 4.05 (s, 2H, CH_2-1), 6.95–7.14 (m, 4H, ArH); ^{13}C NMR (300 MHz, $CDCl_3$) δ: 31.0 (CH_2-4), 46.6 (CH_2-1), 52.0 (OCH_3), 55.3 (CH-3), 125.9 (CH), 126.1 (CH), 126.2 (CH), 128.8 (CH), 132.4 (2C), 172.9 (*C*OOCH$_3$); APIES positive *m*/*z* (%): 214 (100) [M^++ Na^+], 192 (52) [MH^+].

4.1.2. (*S*)-Methyl-2-(2-bromoacetyl)-1,2,3,4-tetrahydro-isoquinoline-3-carboxylate (4a,4b). Under N_2, bromoacetyl bromide (0.045 mL, 0.52 mmol, 1 equiv) was added to a stirred solution of THIQ methyl ester hydrochloride, **3** (118 mg, 0.52 mmol, 1 equiv) and Et_3N (0.11 mL, 0.78 mmol, 1.5 equiv) in anhydrous CH_2Cl_2 (4 mL) at 0 °C and then, stirred at room temperature for 3 h. The reaction mixture was washed with saturated $NaHCO_3$ solution, H_2O and brine, dried over Na_2SO_4, filtered and evaporated under reduced pressure. The residue was purified by flash chromatography (CH_2Cl_2/EtOAc, 9.6:0.4) to afford 105 mg of bromoacetamide-THIQ derivative **4** (65%) as a mixture of rotamers in a 2:1 ratio of **4a**:**4b** rotamers.

^{1}H NMR (400 MHz, $CDCl_3$) δ: 3.15 (dd, J=16.0, 6.0 Hz, 1H, CH_2a-4, rotamer-4a), 3.26 (dd, J=16.0, 4.0 Hz, 1H, CH_2b-4, rotamer-4a), 3.29–3.42 (m, 2H, CH_2-4, rotamer-4b), 3.62 (s, 3H, OCH_3, rotamer-4b), 3.63 (s, 3H, OCH_3, rotamer-4a), 3.93 (m, 2H, CH_2Br, rotamer-4b), 4.0 (d, J=10.8 Hz, 1H, CH_2a–Br, rotamer-4a), 4.06 (d, J=10.8 Hz, 1H, CH_2b–Br, rotamer-4a), 4.53 (d, J=17.6 Hz, 1H, CH_2a-1, rotamer-4b), 4.78 (s, 2H, CH_2-1, rotamer-4a), 4.95 (d, J=17.6 Hz, 2H, CHb-1 and CH-3, rotamer-4b), 5.37 (dd, J=6.0, 4.0 Hz, 1H, CH-3, rotamer-4a), 7.10–7.30 (m, 4H, ArH); ^{13}C NMR (100 MHz, $CDCl_3$) δ: 26.1 (CH_2Br), 30.5 (CH_2-4), 46.2 (CH_2-1), 52.0 (OCH_3), 52.4 (CH-3), 126.0 (CH), 126.8 (CH), 127.0 (CH), 128.3 (CH), 131.4 (C), 131.8 (C), 166.6 (CO), 170.8 (*C*OOCH$_3$); EIMS *m*/*z* (%): 312 (5) [M^+], 232 (100) [M^+−Br], 190 (75) [M^+−$COCH_2$Br], 146 (88) [M^+−$COCH_2$Br–CH_3], 130 (79).

4.1.3. (*S*)-2,3,11,11a-Tetrahydro-2-(2′-(pyrrolidin-3′-yl)ethyl)-6*H*-pyrazino-[1,2-*b*]isoquinoline-1,4-dione (5) and its 2-(2′-piperidin-3′-yl)ethyl homologue (6). Under N_2, a stirred suspension of (*S*)-methyl-2-(2-bromoacetyl)-1,2,3,4-tetrahydro-isoquinoline-3-carboxylate, **4** (100 mg, 0.32 mmol, 1 equiv), 1-(2-aminoethyl)piperidine (0.046 mL, 0.32 mmol, 1 equiv) and anhydrous K_2CO_3 (70 mg) in dry CH_2Cl_2 (6 mL) was refluxed for 4 h. Then, the reaction mixture was cool to room temperature, and washed with H_2O, brine, dried over $NaSO_4$, filtered and evaporated under reduced pressure. The residue was purified by flash chromatography (CH_2Cl_2/MeOH/NH_4OH, 9.6:0.4:1 drop) to obtain 60 mg of compound **6** (57%). The same procedure using 1-(2-aminoethyl)pyrrolidine was accomplished for compound **5** (49 mg, 49%).

Compound **5**. $[\alpha]_D$=−142° (*c* 0.9, EtOH); IR (dry film) ν_{max}: 3470, 2944, 1673, 1456, 1325 cm^{-1}; ^{1}H NMR (300 MHz, $CDCl_3$) δ: 1.70–1.84 (m, 4H, CH_2-5′ and CH_2-6′), 2.50–2.60 (m, 4H, CH_2-4′ and CH_2-7′), 2.71 (t, J=6.5 Hz, 2H, CH_2-2′), 3.01 (dd, J=15.9, 3.4 Hz, 1H, CH_2a-11), 3.43 (dd, J=15.9, 12.4 Hz, 1H, CH_2b-11), 3.50–3.66 (m, 2H, CH_2-1′), 4.19 (s, 2H, CH_2-3), 4.16–4.25 (m, 1H, CH-11a), 4.33 (d, J=17.1 Hz, 1H, CH_2a-6), 5.29 (d, J=17.1 Hz, 1H, CH_2b-6), 7.10–7.30 (m, 4H, ArH); ^{13}C NMR (75 MHz, $CDCl_3$) δ: 23.4 (CH_2-5′ and CH_2-6′), 33.5 (CH_2-11), 43.89 (CH_2-6), 44.9 (CH_2-1′), 50.3 (CH_2-3), 53.0 (CH_2-4′and CH_2-7′), 54.1 (CH_2-2′), 55.5 (CH-11a), 126.2 (CH), 126.9 (CH), 128.6 (2CH), 131.2 (C-10a), 132.4 (C-6a), 162.6 (C-1), 164.8 (C-4); LSIMS *m*/*z* 314 [MH^+].

Compound **6**. $[\alpha]_D^{25}$ −156° (*c* 0.8, EtOH); IR (dry film) ν_{max}: 3486, 2934, 1661, 1470, 1325 cm^{-1}; ^{1}H NMR (300 MHz, $CDCl_3$) δ: 1.34–1.45 (m, 1H, H-6′), 1.50–1.60 (m, 4H, CH_2-5′and CH_2-7′), 2.35–2.48 (m, 4H, CH_2-4′ and CH_2-8′), 2.54 (t, J=6.3 Hz, 2H, CH_2-2′), 3.01 (dd, J=16.0, 12.4 Hz, 1H, CH_2a-11), 3.40 (dd, J=16.0, 3.7 Hz, 1H, CH_2b-11), 3.44–3.54 (m, 1H, CH_2a-1′), 3.58–3.68 (m, 1H, CH_2b-1′), 4.15 (s, 2H, CH_2-3), 4.18–4.24 (m, 1H, CH-11a), 4.30 (d, J=17 Hz, 1H, CH_2a-6), 5.25 (d, J=17 Hz, 1H, CH_2b-6), 7.12–7.30 (m, 4H, ArH); ^{13}C NMR (75 MHz, $CDCl_3$) δ: 24.1 (CH_2-6′), 25.8 (CH_2-5′ and CH_2-7′), 33.4 (CH_2-11), 43.1 (CH_2-1′), 43.7 (CH_2-6), 50.3 (CH_2-3), 54.5 (CH_2-4′ and CH_2-8′), 55.5 (CH-11a), 55.7 (CH_2-2′), 126.1 (CH), 126.8 (CH), 128.6 (2CH), 131.3 (C-10a), 132.4 (C-6a), 162.6 (C-4), 164.73 (C-1); HRMS (EI) *m*/*z* calcd for $C_{19}H_{25}N_3O_2$ [M^+] 327.1947, found 327.1943.

4.2. Crystal structure determination of 6·HCl·2H$_2$O

A colourless lath of 0.79×0.23×0.07 mm size was mounted on a glass fibre and transferred to the diffractometer (orthorhombic, $P2_12_12_1$, a=7.9742(16), b=12.875(3), c=19.791(4) Å, V=2032.0(7) Å^3, Z=4, ρ_{calcd}=1.307 g cm^{-3}, θ_{max}=24.98, Mo Kα, λ=0.71073 Å, ω-scan, diffractometer Nonius CAD4, T=293(2) K, 5953 reflections collected of which 3557 were independent, R_{int}=0.052). The structure was solved by direct methods and refined anisotropically on F^2 (SHELXS-97 and SHELXL-97, Sheldrick, University of Göttingen, 1997). The water hydrogen atoms were located in a difference Fourier synthesis and refined with restrained O–H bond length. Other hydrogen atoms were included using a riding model. The absolute structure was determined (Flack parameter 0.03(13); Flack, H. D. *Acta Crystallogr., Sect. A*, **1983**, *39*, 876).

4.3. Theoretical calculations

All the calculations have been performed with the GAUSSIAN 03 suit of programs.[15] The geometries of all

the relevant points along the reaction path for the alkylation–cyclisation (**R**, **TS** and **P**), have been optimised at PM3, RHF/6-31G(d), RB3LYP/6-31G(d) and RB3LYP/6-31++G(d,p) levels of theory. Vibrational frequencies for the optimised structures were computed to evaluate the zero-point energies (ZPE) as well as to confirm the nature of the singular points along the potential energy surface. The stationary points have been identifies as a minimum with no imaginary frequencies, or as a maximum characterised by the existence of only one imaginary frequency in the normal mode coordinate analysis. Transition state structures were located until the Hessian matrix had only one imaginary eigenvalue, and the transition states were also confirmed by animating the negative eigenvectors coordinate with a visualisation program and internal reaction coordinate (IRC) calculations.[16,17] RHF/6-31G(d) IRC calculations were performed on the transition state (**TS**) structure to check that the **TS** structure leads to reactants and to the reaction product (forward and reverse directions of the reaction path). IRC calculations steps 4 points in cartesians coordiantes in the forward direction and 4 points in the reverse direction, in steps of 0.3 amu$^{1/2}$ bohr along the path were carried out. Correlation effects were included using density functional theory (DFT) with the Becke3-Lee-Yang-Parr (B3LYP)[18] functional. The B3LYP method gave reasonable relative energies with diffuse basis sets, and, for example, 6-31+G(d,p) was suggested by Csonka,[19] and Hoffman and Rychlewsky[20] as sufficient but still computationally economical choice. However, regarding the basis set superimposition errors (BSSEs), the basis set should be extended to 6-31++G(d,p).[20]

Molecular geometry optimisations for the conformation obtained from X-ray neutralised with a chloride were performed at two levels of theory, RHF/3-21G and RB3LYP/6-31G(d). The electronic study of this conformation was carried out using molecular electrostatic potentials (MEPs).[21,22] MEPs were calculated using RB3LYP/6-31G(d) wave function from Gaussian 03 program. The Molekel program[23] was used as the graphic interface to visualise the MEPs.

Acknowledgements

The authors want to thank the Fundación Ana y José Royo for postdoctoral fellowship to N.C. This work was partially supported by grants from Universidad Nacional de San Luis-Argentina. R.D.E. is member of the Scientific staff of CONICET (Argentina). Lic M.F. Massman originally carried out some calculations reported here and we gratefully acknowledge his contribution to this research.

Supplementary data

Supplementary data associated with this article can be found, in the online version, at doi:10.1016/j.tet.2006.02.065. Crystallographic data (excluding structure factors) for the structure in this paper have been deposited with the Cambridge Crystallographic Data Centre as supplementary publication number CCDC 284187. Copies of the data can be obtained, free of charge, on application to CCDC, 12 Union Road, Cambridge CB2 1EZ, UK [fax: +1 44 1223 336033 or e-mail: deposit@ccdc.cam.ac.uk]. Deposited information necessary to guarantee reproducibility.

Table S2 gives the analytical frequencies of **TS** obtained from RB3LYP/6-31G(d) and RB3LYP/6-31++g(d,p) calculations.

Table S3 gives the RB3LYP/6-31G(d) optimised geometry of compound **6** neutralised with a chloride.

References and notes

1. Bentley, K. W. *Nat. Prod. Rep.* **2005**, *22*, 249.
2. Hamburger, M. *Phytochem. Rev.* **2002**, *1*, 333.
3. Hätzelt, A.; Laschat, S.; Jones, P. G.; Grunenberg, J. *Eur. J. Org. Chem.* **2002**, 3936.
4. Gitto, R.; Caruso, R.; Orlando, V.; Quartarone, S.; Barreca, M. L.; Ferreri, G.; Russo, E.; De Sarro, G.; Chimirri, A. *Il Farmaco* **2004**, *59*, 7.
5. Awad, E. M.; Elwan, N. M.; Hassaneen, H. M.; Linden, A.; Heimgartner, H. *Helv. Chim. Acta* **2001**, *84*, 1172.
6. Elwan, N. M.; Abdelhadi, H. A.; Abdellah, T. A.; Hassaneen, H. M. *Tetrahedron* **1996**, *52*, 3451.
7. Herberich, B.; Kinugawa, M.; Vazquez, A.; Williams, R. M. *Tetrahedron Lett.* **2001**, *42*, 543.
8. Cabedo, N.; Protais, P.; Cassels, B. K.; Cortes, D. *J. Nat. Prod.* **1998**, *61*, 709.
9. Cabedo, N.; Andreu, I.; Ramírez de Arellano, M. C.; Chagraoui, A.; Serrano, A.; Bermejo, A.; Protais, P.; Cortes, D. *J. Med. Chem.* **2001**, *44*, 1794.
10. (a) Pictet, A.; Spengler, T. *Ber.* **1911**, *44*, 2030. (b) Cox, E. D.; Cook, J. M. *Chem. Rev.* **1995**, *95*, 1797.
11. (a) Julian, P.-L.; Karpel, W.-J.; Magnani, A.; Meyer, E.-W. *J. Am. Chem. Soc.* **1948**, *70*, 180. (b) Monsees, A.; Laschat, S.; Kotila, S.; Fox, T.; Würthwein, E.-U. *Liebigs Ann./Recueil.* **1997**, 533.
12. Gois, P. M. P.; Afonso, C. A. M. *Eur. J. Org. Chem.* **2003**, 3798.
13. Chiou, C.-M.; Kang, J.-J.; Lee, S.-S. *J. Nat. Prod.* **1998**, *61*, 46.
14. Suvire, F. D.; Rodriguez, A. M.; Mak, M. L.; Papp, J.; Enriz, R. D. *J. Mol. Struct. (Theochem)* **2001**, *540*, 257.
15. Frisch, M. J.; Trucks, G. W.; Schlegel, H. B.; Scuseria, G. E.; Robb, M. A.; Cheeseman, J. R.; Montgomery, J. A., Jr.; Vreven, T.; Kudin, K. N.; Burant, J. C.; Millam, J. M.; Iyengar, S. S.; Tomasi, J.; Barone, V.; Mennucci, B.; Cossi, M.; Scalmani, G.; Rega, N.; Petersson, G. A.; Nakatsuji, H.; Hada, M.; Ehara, M.; Toyota, K.; Fukuda, R.; Hasegawa, J.; Ishida, M.; Nakajima, T.; Honda, Y.; Kitao, O.; Nakai, H.; Klene, M.; Li, X.; Knox, J. E.; Hratchian, H. P.; Cross, J. B.; Adamo, C.; Jaramillo, J.; Gomperts, R.; Stratmann, R. E.; Yazyev, O.; Austin, A. J.; Cammi, R.; Pomelli, C.; Ochterski, J. W.; Ayala, P. Y.; Morokuma, K.; Voth, G. A.; Salvador, P.; Dannenberg, J. J.; Zakrzewski, V. G.; Dapprich, S.; Daniels, A. D.; Strain, M. C.; Farkas, O.; Malick, D. K.; Rabuck, A. D.; Raghavachari, K.; Foresman, J. B.; Ortiz, J. V.; Cui, Q.; Baboul, A. G.; Clifford, S.; Cioslowski, J.; Stefanov, B. B.; Liu, G.; Liashenko, A.; Piskorz, P.; Komaromi, I.; Martin, R. L.; Fox, D. J.; Keith, T.; Al-Laham, M. A.; Peng, C. Y.; Nanayakkara, A.; Challacombe, M.; Gill, P. M. W.; Johnson, B.;

Chen, W.; Wong, M. W.; Gonzalez, C.; Pople, J. A. *Gaussian 03*, Revision B.05, Gaussian, Inc.: Pittsburgh PA, 2003.
16. Gonzalez, C.; Schlegel, H. B. *J. Chem. Phys.* **1989**, *90*, 2154.
17. Gonzalez, C.; Schlegel, H. B. *J. Chem. Phys.* **1990**, *94*, 5523.
18. Lee, C.; Yang, W.; Parr, R. G. *Phys. Rev. B* **1988**, *37*, 785.
19. Csonka, G. I. *J. Mol. Struct. (Theochem)* **2002**, *584*, 1.
20. Hoffman, M.; Rychlewski, J. *Comput. Meth. Sci. Technol.* **2000**, *6*, 61.
21. Polilzer, P.; Truhlar, D. G. *Chemical Applications of Atomic and Molecular Eletrostatic Potentials*; Plenum: New York, 1991.
22. Greeling, P.; Langenaeker, W.; De Proft, F.; Baeten, A. *Molecular Electrostatic Potentials: Concepts and Aplications*; Theoretical and Computational Chemistry; Elsevier Science B.V.: Amsterdam, 1996; Vol. 3; pp 587–617.
23. Flükiger, P.; Lüthi, H. P.; Portmann, S.; Weber, J. *MOLEKEL 4.0*; Swiss Center for Scientific Computing: Manno, Switzerland, 2000.